



**Health, demographic change and wellbeing  
Personalising health and care: Advancing active and healthy ageing  
H2020-PHC-19-2014  
Research and Innovation Action**



***Deliverable D5.2  
Reactive Planning***

<b>Deliverable due date: 05.2017</b>	<b>Actual submission date: 28.05.2017</b>
<b>Start date of project: February 1, 2015</b>	<b>Duration: 42 months</b>
<b>Lead beneficiary for this deliverable: INRIA</b>	<b>Revision: 1.0</b>
<b>Authors: Paolo Bevilacqua (UNITN), Luigi Palopoli (UNITN), Marco Frego (UNITN)</b>	
<b>Internal reviewer: Daniele Fontanelli (UNITN)</b>	

<b>The research leading to these results has received funding from the European Union's H2020 Research and Innovation Programme - Societal Challenge 1 (DG CONNECT/H) under grant agreement n° 643644.</b>		
<b>Dissemination Level</b>		
<b>PU</b>	Public	<b>X</b>
<b>CO</b>	Confidential, only for members of the consortium (including the Commission Services)	

The contents of this deliverable reflect only the authors' views and the European Union is not liable for any use that may be made of the information contained therein.



# Contents

<b>Executive Summary</b>	<b>3</b>
<b>1 Introduction</b>	<b>7</b>
1.1 Model of the Obstacles: the pedestrians	7
1.1.1 The choice of HSFM: the Headed SFM	7
<b>2 Pedestrians' trajectories</b>	<b>9</b>
2.1 The Headed Social Force Model	10
2.1.1 Force Inputs	11
2.1.2 Torque Input	11
2.2 Description of the approximating model	12
2.3 Synthesis of the short-horizon HSFM model to the two-segments clothoid spline	14
2.4 Validation of the fitted model with respect to the HSFM trajectories	15
<b>3 Reactive Planner</b>	<b>17</b>
3.1 Assumption on the motion	17
3.2 Intersection of trajectories	18
3.3 Bounding boxes, triangles and trees for clothoid splines	18
3.4 The clothoid Tunnel: a clothoid spline with two offsets	19
3.5 The velocity diagram	19
3.6 Local Re-planning	21
3.7 Reactive Re-planning	22
3.8 Group cohesion	23
<b>4 Example</b>	<b>25</b>
<b>5 Link to other packages</b>	<b>27</b>



# Executive Summary

The deliverable D5.2 “Reactive Planning”, due at month 27, presents the research activities and the implementation of the Reactive Planner, as reported in Task 5.2 “Reactive Planning”. The deliverable focuses primarily on Objective 5.2: “Refine high level plans into executable plans that account for the concrete conditions detected on the ground (e.g., presence of people or obstacles) and that respect the user requirements (e.g., need for personal space or of rest)”. We consider the problem of the reactive planning of an optimal trajectory for service robots used for human assistance in complex environments subject to geometric and dynamic constraints. Reactive planning is used, for example, when the senior using the *FriWalk* and following a planned trajectory encounters an unforeseen obstacle. In such a case, a new local trajectory that avoids the obstacle has to be generated, without violating any constraint and preserving optimality of the planned path whenever is possible. The solution herein presented guarantees that the new trajectory re-joins the previously planned one shortly after the obstacle. Moreover, the transition between the old and the new re-planned trajectory is smooth up to the second derivative (curvature), which makes it easy to track and falls in the set of control actions defined in WP2 - “Modelling”. Finally, the solution is efficient and can be implemented in real-time on lean hardware. In order to validate the approach, we show how the re-planning can be executed in a few milliseconds (on a standard machine). The strict adherence to the elementary actions of WP2 guarantees that the planned deviations can be effectively executed by the *FriWalk* using one, or a combination thereof, of the solutions provided in WP6 - “Design of Robotic Personal Devices”. This deliverable is related to Milestone MS9 - “Final release of the components to be integrated in the second prototype and preparation of final clinical validation”.



# Chapter 1

## Introduction

To address the Reactive Planning problem, some basic ingredients has to be introduced. First we consider as the vehicle the ensemble of the *FriWalk* and the assisted person. The motion of the vehicle is executed along a predefined, desired path, while the work of the Reactive Planner is to minimise the local deviations ensuring that the new trajectory joins the previously planned one shortly after the obstacle. The vehicle is required to move on a path with some boundaries and constraints, which restricts the possible trajectories that can be taken. The occasional presence of obstacles, such as slower vehicles, other human beings walking around or bystanders, generate additional geometric and dynamic constraints. We make the following three assumptions: 1. the geometry of the planned path is known by means of the Activity Planner defined in Task 5.1 - “Activity planning”, 2. the vehicle is equipped with a sensing system able to reveal obstacles and anomalous conditions in the surroundings (e.g., crowded areas, people walking in the proximity of the path), as per the work of WP3 - “Perception of Users and Environment”, 3. the trajectory re-planning has to be executed in real-time and adapted every time an unforeseen situation is detected. In addition, we require the use of lean hardware in order to reduce the costs and simplify the system engineering.

### 1.1 Model of the Obstacles: the pedestrians

We assume that the static geometric constraints, known obstacles, constraints on the dynamic of the vehicle, such as the smoothness of the trajectory defined by the work of WP2 - “Modelling” and executed with the guidance solutions of WP6 - “Design of Robotic Personal Devices”, are dealt by the high level planner. Here we focus only on how to re-plan a local deviation of the original trajectory in case of an unforeseen event. A typical case, when the vehicle travels in a public shared space, is the presence of another person that walks inside the sensing range of the available sensors. The basis for modelling the trajectories of human beings around the walker is given by the Social Force Model (SFM) [11, 19, 10], which is widely accepted, and its recent innovation, the Headed Social Force Model (HSFM) [6], developed within the work carried out in the ACANTO WP2.

#### 1.1.1 The choice of HSFM: the Headed SFM

As reported in D2.1, there are several human motion models that can be adopted for this class of problems. The Social Force Model (SFM) [12, 15] is one of the most popular human motion models based on social forces. In the SFM, each individual is assimilated to a point-wise particle subject to social forces. Hence, the pedestrians’ dynamics are described by means of a system of differential equations. The SFM is especially well suited to reproduce individual motion of pedestrians in high-density scenarios (crowd), as well as the interactions occurring among pedestrians. The potential of the SFM, and in general of models based on social forces, in providing realistic representations of crowd behaviours has been widely acknowledged [11, 19, 10].

Due to this, the original formulation of the SFM has been successively refined in the literature. For example, in [13] the authors propose an alternate version considering both relative positions and velocities, which works particularly well for low density cases. Relative velocities between pedestrians are instead considered in [20], while [17] uses pedestrians' absolute velocities to govern the user head-on interactions.

The different versions of the SFM have not explicitly modelled the dynamics of the pedestrians' heading so far. In the literature contributions previously reviewed, a person is supposed to be able to move freely in any direction at any time. On the contrary, empirical evidence shows that, most of the time, pedestrians tend to move forward, i.e. their velocity vector is most often aligned with their heading, due to the biomechanics of humans. This phenomenon has been observed by several studies [2, 1, 7], which come to the conclusion that a nonholonomic model may be more appropriate to describe human motion in many cases.

For instance, unicycle-like or car-like models, widely used in the mobile robotics field, are able to accurately reproduce goal-oriented locomotion of an individual moving in free space [2]. Moreover, the adoption of such models in [1] allow to give a nice interpretation of the mechanism underlying the formation of human trajectories (namely, the minimisation of the time derivative of the path curvature, the jerk).

In D2.2 the ACANTO paper [6] has been subsumed. In that paper the Headed Social Force Model (HSFM) is introduced, in order to enhance the traditional SFM by explicitly accounting for the pedestrians' heading. To this end, the motion of each individual is described by means of a dynamic model similar to that adopted in [14] for generating biologically-inspired robot trajectories. In low density scenarios, the pedestrians' motion is as smooth as possible, consistently with what is empirically observed [16]. In these circumstances, lateral motions are avoided because individuals walk ahead most of the time. On the contrary, in crowded or cluttered environments, the interaction among pedestrians, as well as between pedestrians and the environment, is stronger and determines most of the pedestrians' trajectories. Moreover, the novel introduction of an additional force reproduces the behaviour of people intentionally walking together as a single group (e.g., friends or colleagues). This is achieved by defining a desired region (depending on both the position and the heading of the pedestrians) within which the group is expected to lie as a result of the social ties among group members. The new force term is designed to drive the individuals back into the region whenever they leave it. This allows the model to rule out trajectories which do not facilitate social interaction, such as pedestrians arranged in a single line or spread over large areas, a behaviour instead observed with the classic SFM. The preference towards nonholonomic motions in the proposed model does not compromise its ability to reproduce individuals moving in groups. Overall, considering the pedestrians' heading enhances the fidelity of the model in two ways. Whenever nonholonomic motion patterns naturally arise, the generated trajectories resemble more closely those empirically observed. Typical examples include people walking in open spaces or reaching close targets. More generally, accounting explicitly for the pedestrians' heading helps to increase the regularity of the trajectories, resulting in fewer abrupt changes of direction and a reduced number of collisions.

## Chapter 2

# Pedestrians' trajectories

We noticed that the improvements from SFM to HSFM lead naturally to trajectories that are concatenations of clothoid curves as the underlying model is the car-like and the velocity is considered (piecewise) constant. This is in perfect alignment with the control manoeuvres of WP2 - “Modelling” and, from a control perspective, with the trajectory generated by the guidance systems developed in WP6 - “Design of Robotic Personal Devices”. However, the richness of the HSFM does not allow us to directly use it in our reactive planner. The reason is the computational burden of the set of differential equations that govern the human motion model and the various constraints among the social forces. In fact, a simple (but quick) integrator as a one step Euler method does not converge in all cases. Hence the computation has to rely on a more robust Runge-Kutta scheme of order 4, which is of course slower. The computational time is only about a fraction of second, but too slow for our purposes.

Being this model infeasible for real-time purposes, we had to switch to a simplified version of the model. This is not a limitation because the walker can sense a moving obstacle in front of it only within a range of about 3 meters. For such ranges, we have observed the trajectories produced by the HSFM and they can be approximated by the concatenation of two clothoid arcs: first a curved arc that produces the rotation from the initial orientation to the desired end point; then a second clothoid arc given by a straight line toward the endpoint of the trajectory. Some examples of those trajectories produced by the HSFM model are depicted in Figure 2.1. The trajectories connect an initial point  $P_0$  with a specified orientation (an initial angle) to many different final target positions displaced on a half circle of radius 3 meters. To let the deliverable be self-contained, the next section reports a summary of the HSFM (see D2.2 for additional details).

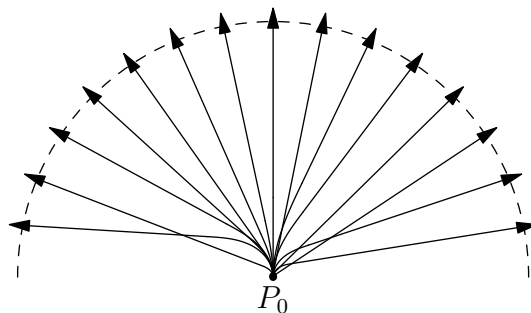


Figure 2.1: Examples of short-horizon trajectories produced by the HSFM model for a free walk in an open space. Different parameters have been changed, taking into account different physical characteristics of the pedestrians. All trajectories origin at point  $P_0$  with the same initial orientation and end at different target positions after a horizon of about 3 meters.

## 2.1 The Headed Social Force Model

We present now the mathematical details of the proposed Headed Social Force Model. Consider a system of  $n$  pedestrians moving in a 2D environment. The  $i$ -th individual,  $i = 1, \dots, n$ , is assimilated to a particle with mass  $m_i$ , whose position and velocity, expressed in a global reference frame, are denoted by  $\mathbf{r}_i = [x_i, y_i]^\top$  and  $\mathbf{v}_i = [\dot{x}_i, \dot{y}_i]^\top$ , respectively. The equations of motion are

$$\begin{aligned}\dot{\mathbf{r}}_i &= \mathbf{v}_i, \\ \dot{\mathbf{v}}_i &= \frac{1}{m_i} \mathbf{u}_i,\end{aligned}$$

where  $\mathbf{u}_i$  represents the social force driving the  $i$ -th particle. In order to include the pedestrians' heading into the model, it is convenient to attach a body frame to each individual, i.e. a reference frame centred at the pedestrian's position and whose  $x$ -axis is aligned with the pedestrian's forward direction of motion. Let  $\mathbf{q}_i = [\theta_i, \omega_i]^\top$  be the vector containing the heading  $\theta_i$  (angle between the  $x$ -axis of the body frame and that of the global reference frame) and the angular velocity  $\omega_i = \dot{\theta}_i$  of the  $i$ -th pedestrian. Denote by  $\mathbf{v}_i^B = [v_i^f, v_i^o]^\top$  the velocity vector expressed in the body frame. The components  $v_i^f$  and  $v_i^o$  of vector  $\mathbf{v}_i^B$  correspond to the projection of the velocity vector  $\mathbf{v}_i$  along the forward direction and the orthogonal direction, respectively. Clearly,  $\mathbf{v}_i = \mathbf{R}(\theta_i) \mathbf{v}_i^B$ , where the rotation matrix  $\mathbf{R}(\theta_i)$  is defined as

$$\mathbf{R}(\theta_i) = \begin{bmatrix} \cos(\theta_i) & -\sin(\theta_i) \\ \sin(\theta_i) & \cos(\theta_i) \end{bmatrix} \doteq \begin{bmatrix} \mathbf{r}_i^f & \mathbf{r}_i^o \end{bmatrix}.$$

Then, similarly to [14], the human locomotion model can be written as

$$\dot{\mathbf{r}}_i = \mathbf{R}(\theta_i) \mathbf{v}_i^B, \quad (2.1)$$

$$\dot{\mathbf{v}}_i^B = \frac{1}{m_i} \mathbf{u}_i^B, \quad (2.2)$$

$$\dot{\mathbf{q}}_i = \mathbf{A} \mathbf{q}_i + \mathbf{b}_i u_i^\theta, \quad (2.3)$$

where

$$\mathbf{A} = \begin{bmatrix} 0 & 1 \\ 0 & 0 \end{bmatrix}, \quad \mathbf{b}_i = \begin{bmatrix} 0 \\ \frac{1}{I_i} \end{bmatrix}, \quad (2.4)$$

and  $I_i$  denotes the moment of inertia of pedestrian  $i$ . In model (2.1)-(2.3), the inputs are  $\mathbf{u}_i^B = [u_i^f, u_i^o]^\top$ , whose entries are the forces acting along the forward direction and the orthogonal direction, respectively, as well as the torque  $u_i^\theta$  about the vertical axis. Notice that such a model is indeed unconstrained. However, if  $v_i^o(0) = 0$  and  $u_i^o(t) = 0$ , for all  $t$ , the dynamic unicycle model is recovered. In general, whenever  $v_i^o = 0$ , the model features a nonholonomic behaviour, the velocity vector being aligned with the pedestrian's heading.

The basic idea of the HSFM is to compute the model inputs  $u_i^f$ ,  $u_i^o$  and  $u_i^\theta$  on the basis of the the forces resulting from the traditional SFM. To this purpose, the total force  $\mathbf{f}_i$  that acts on the  $i$ -th pedestrian according to [11] is decomposed as

$$\mathbf{f}_i = \mathbf{f}_i^0 + \mathbf{f}_i^e. \quad (2.5)$$

The first term

$$\mathbf{f}_i^0 = m_i \frac{\mathbf{v}_i^d - \mathbf{v}_i}{\tau_i} \quad (2.6)$$

accounts for the pedestrian's desire to move with a given velocity vector  $\mathbf{v}_i^d$ . In (2.6), the characteristic time  $\tau_i > 0$  is a parameter determining the rate of change of the velocity vector. The force

$$\mathbf{f}_i^e = \mathbf{f}_i^p + \mathbf{f}_i^w \quad (2.7)$$

accounts for the pedestrians' interaction. The terms  $\mathbf{f}_i^p$  and  $\mathbf{f}_i^w$  represent the repulsive forces exerted on individual  $i$  by the other pedestrians and by possible obstacles present in the environment (e.g., walls), respectively. The expressions of  $\mathbf{f}_i^p$  and  $\mathbf{f}_i^w$  are simply given by linear combination of the relations defined for the standard SFM and define the effects of other pedestrians on individual  $i$  and the repulsive effects of obstacles or boundaries such as walls on individual  $i$ , respectively, i.e.

$$\mathbf{f}_i^p = \sum_{j \neq i} \mathbf{f}_{ij}^{\text{soc}} + \mathbf{f}_{ij}^{\text{ph}} \quad \text{and} \quad \mathbf{f}_i^w = \sum_b \mathbf{f}_{ib}^{\text{soc}} + \mathbf{f}_{ib}^{\text{ph}}.$$

### 2.1.1 Force Inputs

The inputs of the HSFM are computed from  $\mathbf{f}_i^0$  and  $\mathbf{f}_i^e$  as follows. The input vector  $\mathbf{u}_i^B$  includes the forces acting along the pedestrian's forward direction and the orthogonal direction. Given the total social force  $\mathbf{f}_i$ , a natural choice for computing  $u_i^f$  is to project  $\mathbf{f}_i$  along the forward direction. In order to avoid sideward motions if not strictly needed, the component  $u_i^o$  is computed by projecting the interaction force  $\mathbf{f}_i^e$  (possibly scaled), along the orthogonal direction. Finally, in order to drive to zero the sideward velocity  $v_i^o$  when the sideward force is zero, a damping term proportional to  $v_i^o$  is added to  $u_i^o$ . Hence, the model inputs  $u_i^f$  and  $u_i^o$  are computed as

$$u_i^f = (\mathbf{f}_i^0 + \mathbf{f}_i^e)^\top \mathbf{r}_i^f, \quad (2.8)$$

$$u_i^o = k^o (\mathbf{f}_i^e)^\top \mathbf{r}_i^o - k^d v_i^o, \quad (2.9)$$

where  $k^o > 0$  and  $k^d > 0$ .

### 2.1.2 Torque Input

The input  $u_i^\theta$  represents the torque about the vertical axis which drives the dynamics of the pedestrian's heading. This term is designed on the basis of the force  $\mathbf{f}_i^0$  defined in (2.6). Denote by  $f_i^0$  and  $\theta_i^0$  the magnitude and the phase in the global reference frame of  $\mathbf{f}_i^0$ . Notice that both quantities are in general time-varying. The input  $u_i^\theta$  is computed as

$$u_i^\theta = -k^\theta (\theta_i - \theta_i^0) - k^\omega \omega_i. \quad (2.10)$$

The parameters  $k^\theta$  and  $k^\omega$  are designed in order to achieve suitable dynamics of the heading. It can be easily verified that, with  $u_i^\theta$  defined as in (2.10), the orientation error  $\tilde{\theta}_i \doteq \theta_i - \theta_i^0$  evolves according to the dynamic model

$$\ddot{\tilde{\theta}}_i + \frac{k^\omega}{I_i} \dot{\tilde{\theta}}_i + \frac{k^\theta}{I_i} \tilde{\theta}_i = -\frac{k^\omega}{I_i} \dot{\theta}_i^0 - \ddot{\theta}_i^0. \quad (2.11)$$

A possible design procedure is to select the values of  $k^\theta$  and  $k^\omega$  on the basis of the desired poles  $\lambda_1$  and  $\lambda_2$  of the dynamic system (2.11). For the ACANTO model, real poles are considered, so that  $\lambda_2 = \alpha \lambda_1 < 0$ , for some  $\alpha > 1$ . In turn, the dominant pole  $\lambda_1$  is selected as a function of  $f_i^0$

$$\lambda_1 = -\sqrt{\frac{k^\lambda f_i^0}{\alpha}},$$

where  $k^\lambda > 0$  is used to tune the dominant time constant of system (2.11). The corresponding expressions of  $k^\theta$  and  $k^\omega$  are then

$$k^\theta = I_i k^\lambda f_i^0, \quad k^\omega = I_i (1 + \alpha) \sqrt{\frac{k^\lambda f_i^0}{\alpha}}. \quad (2.12)$$

The choice of time-varying poles allows one to modulate the responsiveness of the system with the intensity of the driving force  $\mathbf{f}_i^0$ . The underlying idea is that the more authoritative the  $\mathbf{f}_i^0$ , the faster the change in the pedestrian's heading. In this way, the heading convergence rate is proportional to  $f_i^0$ .

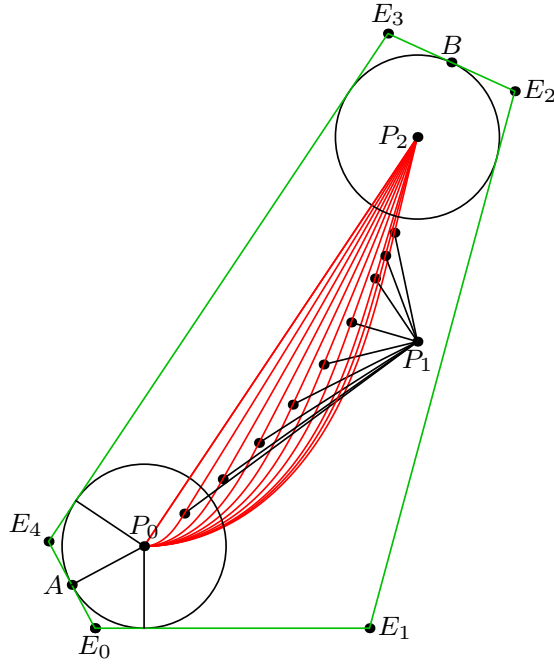


Figure 2.2: Ten different two-segments clothoid splines that join with curvature continuity a starting point  $P_0$  and reach a final (target) point  $P_2$ . The points labelled with  $P_1$  are the connection points between first and second segment, respectively proper clothoid and straight line. The splines are modelled with ten different values of the percentage  $p$  ranging from 0% to 100% with step 10%. In green it is shown a bounding polygon  $E_0E_1 \dots E_4$  that contains all the possible splines with a constant offset.

## 2.2 Description of the approximating model

In this section we describe the construction of the two-segment clothoid spline that approximates the HSFM trajectory. To approximate them in order to avoid the numerical integration, we have carried out several simulations to derive the sensitivity of the numerous parameters of the HSFM model. The result of the simulation is that the parameters of the model described in Section 2.1 that have greater influence on the shape of the trajectory are the reaction time of the pedestrian  $\tau$  which is slower for young people and higher for more aged people; the parameter  $k^o$  that models the orthogonal force; the value  $k^\lambda$  that tunes the time constants and  $\alpha$  which models the ratio of the poles of the dynamical system, resulting in a loose or sharp curvature profile of the trajectory.

It is not possible to extract *a priori* data relative to the number of elementary arcs that build an HSFM trajectory, however experimental evidence shows that two arcs give sufficient accuracy. The first arc is a proper clothoid, whereas the second arc is a straight line. The connection between them is done enforcing curvature continuity, so that jumps and corners are avoided. The construction of the two-segment clothoid spline that approximates the previously described HSFM trajectories can now be tackled (see Figure 2.2 for reference). The geometric construction requires to find the parameters of two clothoids that meet in the middle at point  $P_1$ , such that the second segment is a straight line. The clothoid curve [3] is defined as

$$\begin{aligned} x(s) &= x_0 + sX_0(\kappa' s^2, \kappa s, \theta), \\ y(s) &= y_0 + sY_0(\kappa' s^2, \kappa s, \theta), \end{aligned} \quad (2.13)$$

where

$$\begin{aligned} X_n(a, b, c) &= \int_0^1 \tau^n \cos\left(\frac{a}{2}\tau^2 + b\tau + c\right) d\tau, \\ Y_n(a, b, c) &= \int_0^1 \tau^n \sin\left(\frac{a}{2}\tau^2 + b\tau + c\right) d\tau. \end{aligned} \quad (2.14)$$

It is worthwhile to note that for a clothoid, the tangent takes the form  $\psi(s) = \frac{1}{2}\kappa's^2 + \kappa s + \theta$ . The relation between  $\psi$  and the curvature  $k$  is differential, i.e.,  $\psi'(s) = k(s) = \kappa + \kappa's$ , which points out a crucial feature: the curvature is a linear (affine) function of the arc length  $s$ . Our method seeks the path that joins two positions  $P_0$  and  $P_2$ , respectively the initial and final point. At  $P_0$  we specify the  $xy$ -position, that is,  $P_0 = (x_0, y_0)$ , and an initial angle  $\theta_0$ . The second segment must be a straight line that meets the given final point  $P_2 = (x_2, y_2)$ , hence the curvatures  $\kappa'$  and  $\kappa$  must be zero. To model the different shapes of the resulting spline as in Figure 2.2, we use a tuning parameter  $p \in (0, 1)$  and define the length  $L_2$  of the straight line as a percentage of the Euclidean distance between  $P_0$  and  $P_2$ . In other words we set  $L_2 = p \cdot \text{dist}(P_0, P_2)$ . The tuning coefficient  $p$  is assigned on the basis of the physical characteristics of the modelled pedestrian. The choice of  $p$  is discussed in the sequel on the basis of the simulation of many trajectories by different pedestrians. At the joining point  $P_1$ , which is unknown, we require  $G^2$  geometric continuity up to the second derivative, in other words the tangent and the curvature of the two arcs should meet continuously in  $P_1$ . This results in additional constraints. The nonlinear system to be solved is therefore

$$x_1 = x_0 + L_1 X_0(\kappa' L_1^2, \kappa_0 L_1, \theta_0) \quad (2.15)$$

$$y_1 = y_0 + L_1 Y_0(\kappa' L_1^2, \kappa_0 L_1, \theta_0) \quad (2.16)$$

$$\theta_1 = \frac{1}{2}\kappa' L_1^2 + \kappa_0 L_1 + \theta_0 \quad (2.17)$$

$$\kappa_1 = \kappa' L_1 + \kappa_0 = 0 \quad (2.18)$$

$$x_2 = x_1 + L_2 X_0(0, 0, \theta_1) \quad (2.19)$$

$$y_2 = y_1 + L_2 Y_0(0, 0, \theta_1) \quad (2.20)$$

$$\theta_2 = \theta_1 \quad (2.21)$$

$$\kappa_2 = 0 \quad (2.22)$$

where the subscript  $i$  for  $i = 0, 1, 2$  refers to a condition relative to the point  $P_i$ , the lengths of the two arcs is modelled with  $L_1$  and  $L_2$  respectively. This nonlinear system of equations is a particular case of the general  $G^2$  Hermite Interpolation Problem with clothoids, for which there is no general solution available yet. However this particular form allows us to find a solution by means of the solution of the  $G^1$  Hermite Interpolation Problem with clothoids, [3]. In practise this method solves all the previous equations but (2.18) and yields the unknowns  $L_1$ ,  $\kappa'$  and  $\kappa_0$  as a function of  $\theta_1$ . The missing equation can be viewed as a function of the unknown parameter  $\theta_1$  resulting from the  $G^1$  solution: we can write it as  $h(\theta_1) = 0$ , where

$$h(\theta_1) = \kappa'(\theta_1)L_1(\theta_1) + \kappa_0(\theta_1) = 0 \quad (2.23)$$

This means that having the  $G^1$  solution, we can write Equation (2.18) as a function of one variable  $\theta_1$  as in (2.23). Thus it can be solved for example with the Newton method in few iterations. In summary, the solution strategy calls first the  $G^1$  algorithm of [3] which returns  $L_1$ ,  $\kappa'$  and  $\kappa_0$  (and their derivatives) as a function of  $\theta_1$ . The second step is to find, via the Newton method, the value of  $\theta_1$  that solves (2.23). At convergence, we have a solution of the nonlinear system. Experimental evidence show that the problem at hand is well posed so that in most cases few iterations of the Newton method are enough.

With this technology we can approximate a short-horizon trajectory of the HSMF model with a simple two-segments spline of clothoids. The different shapes of this spline are created varying the percentage parameter  $p$

$d$	# monom.
0	1
1	6
2	21
3	56
4	126

Table 2.1: Number of monomials for a multivariate polynomial of degree  $d$  with  $n = 5$  variables.

discussed above, which contains the physical information of the pedestrian. The synthesis of  $p$  from the HSFM parameters is the topic of the next paragraph.

### 2.3 Synthesis of the short-horizon HSFM model to the two-segments clothoid spline

In the previous paragraph we showed how to construct the simplified two-segments clothoid spline that approximates a short-horizon HSFM trajectory. We discuss now how to synthesise the four sensitive HSFM parameters  $\tau$ ,  $k^o$ ,  $k^\lambda$  and  $\alpha$  that characterise a specific pedestrian. The idea is to fit the percentage parameter  $p$  to a large number of trajectories generated on a fine grid of possible values  $\tau$ ,  $k^o$ ,  $k^\lambda$  and  $\alpha$ . The final point is also varied: the trajectory goes from the origin (with fixed angle  $\theta_0 = 0$ ) to a point on the half circle of radius 3 meters centred at the origin. The ending point is modelled with  $(x_2, y_2) = 3(\cos(\theta_2), \sin(\theta_2))$  for  $\theta_2 \in (-\frac{\pi}{2}, \frac{\pi}{2})$ . Because of the symmetry of the problem, we considered only points in the first quadrant, that is for  $\theta_2 \in [0, \frac{\pi}{2})$ .

The ranges of the HSFM parameters considered is the following:

- $\tau$  is discretised from  $\frac{2}{N}$  to 2 with intervals of width  $\frac{2}{N}$ .
- $k^o$  is discretised from  $\frac{5}{N}$  to 5 with intervals of width  $\frac{5}{N}$ .
- $k^\lambda$  goes from  $\frac{1}{2N}$  to  $\frac{1}{2}$  with step  $\frac{1}{2N}$ .
- $\alpha$  takes two values 3 (sharp turns) and 5 (smooth turns).
- $\theta_2$  is discretised from 0 to  $\frac{\pi}{2} - \frac{\pi}{20}$  with step  $\frac{\pi}{20}$ .
- $N = 20$ , which yields a total of  $N^4 = 160.000$  trajectories.

Each of the generated trajectories is compared with the simplified clothoid model. We tested for each HSMF trajectory 50 clothoid splines, i.e. we generated a spline for 50 different values of the percentage  $p$  ranging from 50% to 99% with step 1%. Among all those clothoid spline we chose the one that is at minimum distance from that particular HSFM trajectory. The metric used is the Root Mean Square Error (RMSE) based on the Euclidean distance between the HSFM and the clothoid trajectory. In this way we have constructed the discrete map that associates to the vector  $(\tau, k^o, k^\lambda, \alpha)$  the optimal percentage  $p$  in terms of the RMSE error. We can now try to fit this data with a simple function. The fitting function  $\varphi$  is a map  $\varphi : \mathbb{R}^5 \mapsto [0, 1]$  such that  $p = \varphi(\tau, k^o, k^\lambda, \alpha, \theta_2)$ . The functional form of  $\varphi$  is chosen as a multivariate polynomial.

With  $n = 5$  variables and degree  $d$  this polynomial has a lot of monomials even for low degree. In particular the number of monomials is given by the binomial coefficient  $\binom{n+d}{d}$ , thus approximatively  $d^5/120$ . The number of monomials for small degree is contained in the following table. Of course, the higher the degree the higher the precision of the fit, however a large number of monomials is not desirable.

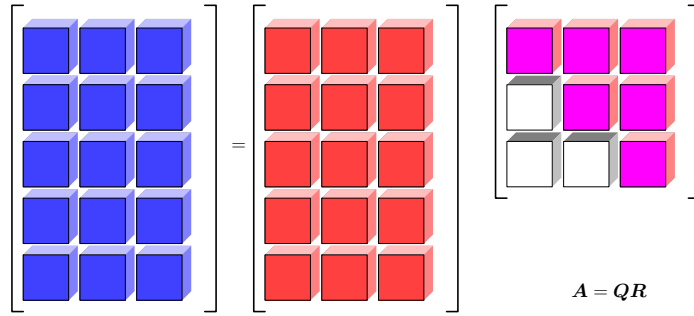
The fitting is performed using least squares techniques based on QR decomposition. We solve thus the problem

$$\min_{\mathbf{x}} \|\mathbf{Ax} - \mathbf{b}\|^2, \quad \mathbf{x} \in \mathbb{R}^{\binom{n+d}{d}}, \quad \mathbf{A} \in \mathbb{R}^{N^4 \times \binom{n+d}{d}}, \quad \mathbf{b} \in \mathbb{R}^{N^4}.$$

The matrix  $\mathbf{A}$  is obtained evaluating for each row the monomials of the fitting polynomial on the particular configuration  $(\tau, \kappa^o, \kappa^\lambda, \alpha, \theta_2)$ , the corresponding right hand side  $\mathbf{b}$  is the optimal value of  $p$  that approximates with clothoids that particular trajectory. The vector  $\mathbf{x}$  contains the coefficients of the monomials that specify the optimal fitting polynomial. The higher the degree  $d$ , the higher the dimension of matrix  $\mathbf{A}$  and hence the harder the optimisation problem.

The QR decomposition of  $\mathbf{A}$  produces a factorisation of the form

$$\mathbf{A} = \mathbf{QR} \in \mathbb{R}^{N^4 \times \binom{n+d}{d}}, \quad \mathbf{Q} \in \mathbb{R}^{N^4 \times \binom{n+d}{d}}, \quad \mathbf{R} \in \mathbb{R}^{\binom{n+d}{d} \times \binom{n+d}{d}}, \quad (2.24)$$



The problem is then easily solved because

$$\|\mathbf{Ax} - \mathbf{b}\|^2 = \|\mathbf{QRx} - \mathbf{b}\|^2 = \|\mathbf{Rx} - \mathbf{Q}^T \mathbf{b}\|^2 \quad (2.25)$$

where we use the fact that  $\mathbf{Q}$  is an orthogonal matrix, e.g.  $\mathbf{QQ}^T = \mathbf{I}$  and the Schwartz inequality of the last step becomes an equality under this hypothesis. Hence the problem is recast to the solution of the smaller linear system  $\mathbf{Rx} - \mathbf{Q}^T \mathbf{b}$  which is also well conditioned. Producing this solution is fast because  $\mathbf{R}$  is an upper triangular matrix.

## 2.4 Validation of the fitted model with respect to the HSFM trajectories

Analysing the problem numerically, it turns out that it is not too bad conditioned and hence we can use a low degree for  $d$ . The fitting with a polynomial of degree  $d = 0, 1, 2, 3, 4$  gives a good result in terms of the RMSE error. Moreover, the price in terms of monomials with respect to the accuracy is acceptable for  $d = 0$ , hence we can approximate the map  $\varphi$  with a constant percentage  $p_{\text{opt}} = 88\%$ . Our tolerance to the error was about 0.5 meters, that is, about the hindrance of a person. Rising the degree produces only a small improvement (see Figure 2.3) in the solution but at the price of a higher number of monomials to be evaluated, thus we choose degree zero. To ensure that the fitting gives the expected results, we validated the choice of  $p_{\text{opt}} = 88\%$  with the set of previously generated HSFM trajectories. The result is shown in Figure 2.3.

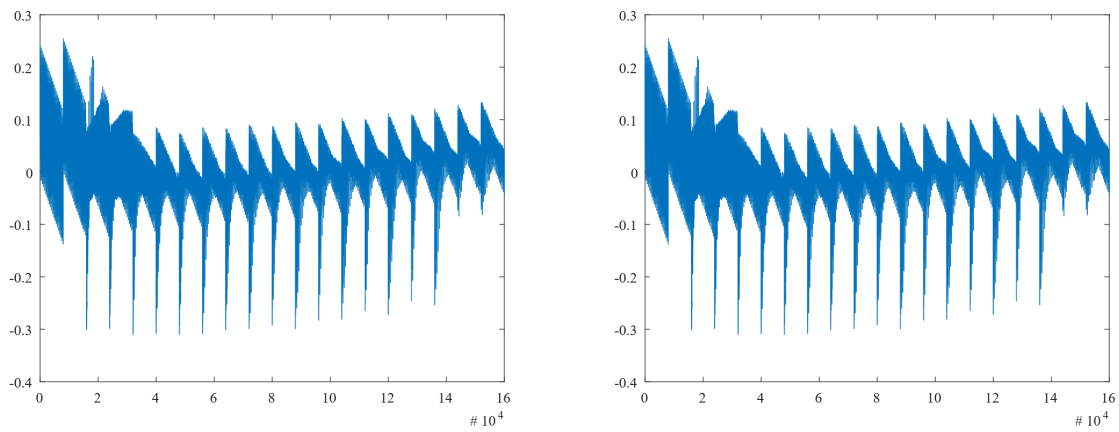


**Figure 2.3:** Left: The RMSE distance (in meters) between the HSFM trajectories and their approximations with the clothoid model with  $p = p_{opt} = 88\%$ . The errors are bounded within 30cm. Moreover, most of the values are bounded within 10cm. Right: same plot but for a polynomial of degree 1, the errors are a bit smaller but the improvement is not that better to justify the choice.

## Chapter 3

# Reactive Planner

### 3.1 Assumption on the motion

We model the human obstacle (pedestrian)  $H$  with constant velocity  $v_{0\alpha}^{(h)}$  according to the ODE

$$h'(t) = v_{0\alpha}^{(h)}, \quad h(0) = h_0, \quad \Rightarrow \quad h(t) = h_0 + v_{0\alpha}^{(h)}t, \quad (3.1)$$

where  $h(t)$  is the curvilinear abscissa of the obstacle (see Figure 3.1). The constant velocity  $v_{0\alpha}^{(h)}$  is chosen randomly inside the interval  $[v_{0\min}^{(h)}, v_{0\max}^{(h)}]$  with known density  $p_\alpha(v_{0\alpha}^{(h)})$ . Its cumulative distribution function is

$$\mathbb{P}(v_{0\alpha}^{(h)} < v) = \int_{v_{0\min}^{(h)}}^v p_\alpha(v_{0\alpha}^{(h)}) dv_{0\alpha}^{(h)}.$$

Being the obstacle not a point, the space around its centre of mass is described with a conservative offset  $\pm\delta_h$  around the abscissa  $h(t)$ , hence the obstacle occupies the interval  $[h(t) - \delta_h, h(t) + \delta_h]$ . We model the *FriWalk*

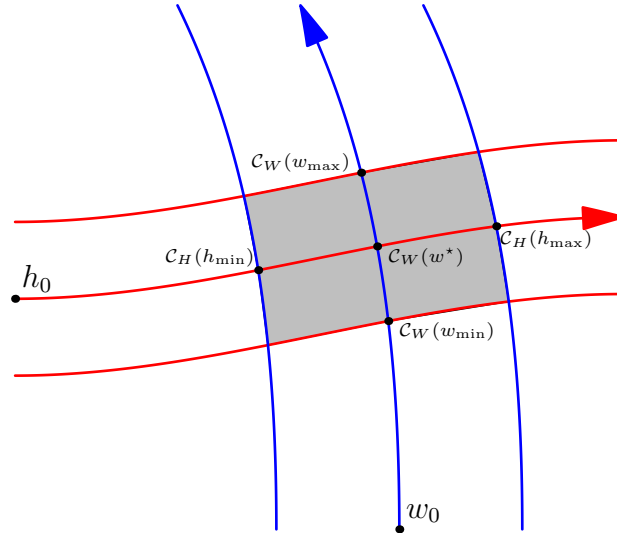


**Figure 3.1:** General scheme for the intersection of the paths of the walker and a pedestrian.  $\mathcal{C}_H(h)$  is the clothoid spline of the human, similarly,  $\mathcal{C}_W(w)$  is the spline of the walker. Both are parametrised by arc length, respectively  $h$  and  $w$ .

$W$  in the same manner of the obstacle. Its curvilinear abscissa is identified with the variable  $w$  (see Figure 3.1).

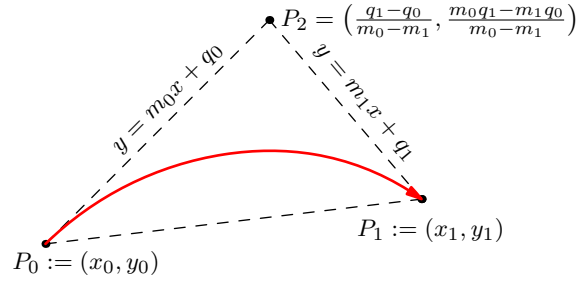


**Figure 3.2:** General scheme for the construction of bounding triangles on a piece of clothoid arc that travels an angle smaller than  $\pi/2$ . The considered portion of clothoid begins in  $P_0$  and ends in  $P_1$ , the geometric intersection of the tangents to the curve in  $P_0$  and  $P_1$  produces the point  $P_2$ . Those three points build the bounding triangle.

### 3.2 Intersection of trajectories

Each agent  $A = \{W, H\}$  moves on a sequence of smoothly joined clothoids, called a clothoid spline. A spline is a parametric curve in the plane  $\mathcal{C}_A(s) = (x(s), y(s))$ . Their hindrance is specified by a constant offset along the spline: the offset for the obstacle is  $\delta_h$ , whereas the offset of the walker is identified with  $\delta_w$ . For the *FriWalk* we do not require any particular form of the spline, and we assume to know it from the high level planner. The form of the spline for the pedestrian can be general (see Figure 3.1), but because of the discussion of the HSFM model, we consider only a spline made up of two segments. To compute the intersection with the path of the walker it is possible to inscribe the clothoid model into a bounding polygon as in Figure 2.2. This allows us to find intersections by employing routines that are based on points and straight segments, which are computationally efficient. Nevertheless, this approach has a main drawback: it can be used to model the pedestrian only. Moreover, it will work only for the two-segment clothoid model, and cannot be easily extended to the case of a more general path, e.g. on a general clothoid spline. Therefore it is convenient to adopt a general scheme, which is flexible to handle both the two-segment spline of the simplified HSFM model and the general clothoid spline of the *FriWalk*. We take advantage of the hierarchic tree structure discussed in the ACANTO paper [5].

### 3.3 Bounding boxes, triangles and trees for clothoid splines

A clothoid spline is made up of several smoothly connected clothoid segments, each clothoid arc has at most one change of sign in the curvature, for  $s = -\kappa_0/\kappa'$ . In other words the spline has  $G^2$  continuity and hence its curvature is a continuous piecewise linear function. If the change of sign in the curvature falls into the interval of the definition of the arc, then we cut the clothoid there in order to have two segments with constant sign curvature. Notice that if both  $\kappa_0 = \kappa' = 0$ , the clothoid boils down to a straight line, while if only  $\kappa' = 0$  the clothoid is an arc of circle. The next step of the segmentation is to divide the previously obtained arcs in equal intervals such that the travelled angle is less than  $\pi/2$ . The idea is to segment the clothoids on the basis of their curvature and then inscribe each portion in a triangle (see Figure 3.2 for reference). To this end, given the  $i$ -th portion of clothoid, we identify the initial point with  $P_{i,0} = (x_{i,0}, y_{i,0})$ , the final point with  $P_{i,1} = (x_{i,1}, y_{i,1})$  at abscissa  $s^*$ , and we show that the third vertex  $P_{i,2} = (x_{i,2}, y_{i,2})$  of the triangle  $P_{i,0}P_{i,1}P_{i,2}$  is given by

$$P_{i,2} = \left( -\frac{q_0 - q_1}{m_0 - m_1}, \frac{m_0q_1 - m_1q_0}{m_0 - m_1} \right), \quad (3.2)$$

where  $m_0 = \tan(\theta_{i,0})$ ,  $q_0 = y_{i,0} - m_0x_{i,0}$ ,  $m_1 = \tan(\theta(s^*))$ ,  $q_1 = y_{i,1} - m_1x_{i,1}$ . The following Theorem ensures that each clothoid can be inscribed in a triangle.

**Theorem 3.3.1.** Consider the clothoid segment obtained as described above, that is, a clothoid of parameters  $\kappa_i, \kappa'_i, \theta_i$  of length  $L_i$  such that the curvature has constant sign on the interval  $(0, L_i)$  and the variation of the angle  $\theta(s)$  is less than  $\pi/2$ , i.e.  $\theta(L_i) - \theta(0) \leq \pi/2$ . Then all the clothoid is contained in the triangle  $P_{i,0}P_{i,1}P_{i,2}$ .

The proof of the theorem, which is based on purely geometric arguments, is not reported for the sake of brevity. Using this approximation, the collision is then detected computing a standard polygon intersection. In the case of a collision, we simply resample some points of the given sequence and repeat the trajectory construction process.

### 3.4 The clothoid Tunnel: a clothoid spline with two offsets

To model the path of the walker or of the pedestrian, we have to consider the clothoid spline with a positive and negative offset given by the physical encumbrance  $\delta_w$  (respectively  $\delta_h$  for the pedestrian). This yields a spline plus two parallel curves at the left and at the right, e.g. see Figure 3.1. It is important to notice that the curve at constant offset from a clothoid is no more a clothoid. Instead, it has the parametric equations

$$X(s) = x(s) + \frac{ay'(s)}{\sqrt{x'(s)^2 + y'(s)^2}}, \quad Y(s) = y(s) - \frac{ax'(s)}{\sqrt{x'(s)^2 + y'(s)^2}}, \quad (3.3)$$

where  $x(s), y(s)$  are the equations of the base curve and  $a$  is the constant offset (positive or negative). We call a clothoid Tunnel the clothoid spline and its two offset curves at distance  $\pm\delta_w$ .

### 3.5 The velocity diagram

In a standard intersection event, the routine for finding the collision will return a sequence of 4 points  $\{A, B, C, D\}$  that are the vertexes of a generalised quadrilateral depicted in Figure 3.3. It is important to underline that not

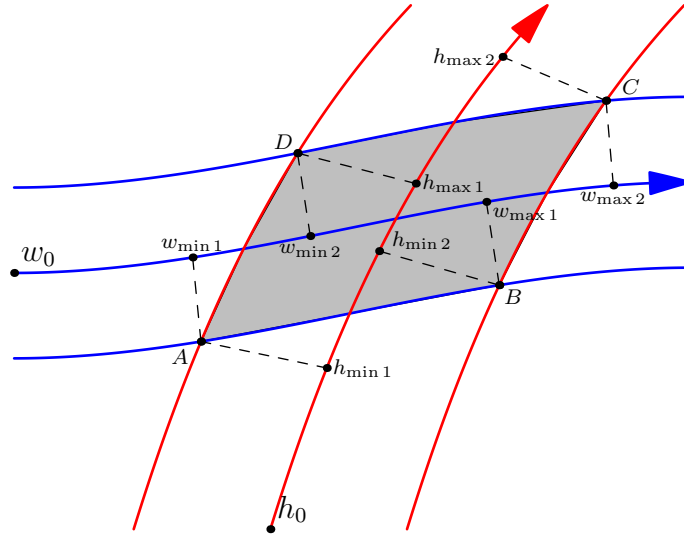


**Figure 3.3:** Projection scheme of the geometric intersection points into the curvilinear abscissas of the walker and of the pedestrian. Those abscissas are then mapped to the corresponding time instants.

every intersection event will have 4 points, for example, if the trajectories are almost tangent, less points will be

found. However, it is always possible to retrieve the standard case identifying the missing points as collapsed points.

With the four intersection points, which are only geometric entities and do not contain dynamic information, we have to compute the curvilinear abscissas of the entry and exit points of the collision zone. They are called  $w_{\min 1}$  and  $w_{\max 2}$  for the walker and  $h_{\min 1}$ ,  $h_{\max 2}$  for the pedestrian (see Figure 3.3). It is easy to compute those abscissas with the routines that handle the clothoid splines and their offsets. In fact it is possible to use a standard Newton method that converges to the solution in few iterations.

It is not enough to consider those coordinates, because of the finite dimension of the agents, therefore we call  $w_{\min} = w_{\min 1} - \delta_w$ ,  $w_{\max} = w_{\max 2} + \delta_w$  and for the pedestrian  $h_{\min} = h_{\min 1} - \delta_h$ ,  $h_{\max} = h_{\max 2} + \delta_h$ . From the curvilinear abscissas to the corresponding travelling time is also an easy step, because by hypothesis the velocities of all agents are constant on each piece of path considered. Those time instants are called accordingly to the name of the abscissas respectively  $t_{w \min}$ ,  $t_{w \max}$ , and the same for the obstacle but with subscript  $h$ . It is convenient to name the time intervals as  $\Delta T_h := [t_{h \min}, t_{h \max}]$  and  $\Delta T_w := [t_{w \min}, t_{w \max}]$ . We declare a collision if and only if the intersection  $\Delta T_h \cap \Delta T_w \neq \emptyset$ .

Those quantities lead naturally to a space-time scheme, that we call velocity diagram, on which the horizontal axis represents the time, the vertical axis the curvilinear abscissa  $w$  of the walker. The velocities, being constant, are thus straight lines from the origin. More interestingly, the collision zone in space and time can be approximated with an octagon, as in the example Figure 3.4. The function that checks if there is a collision is

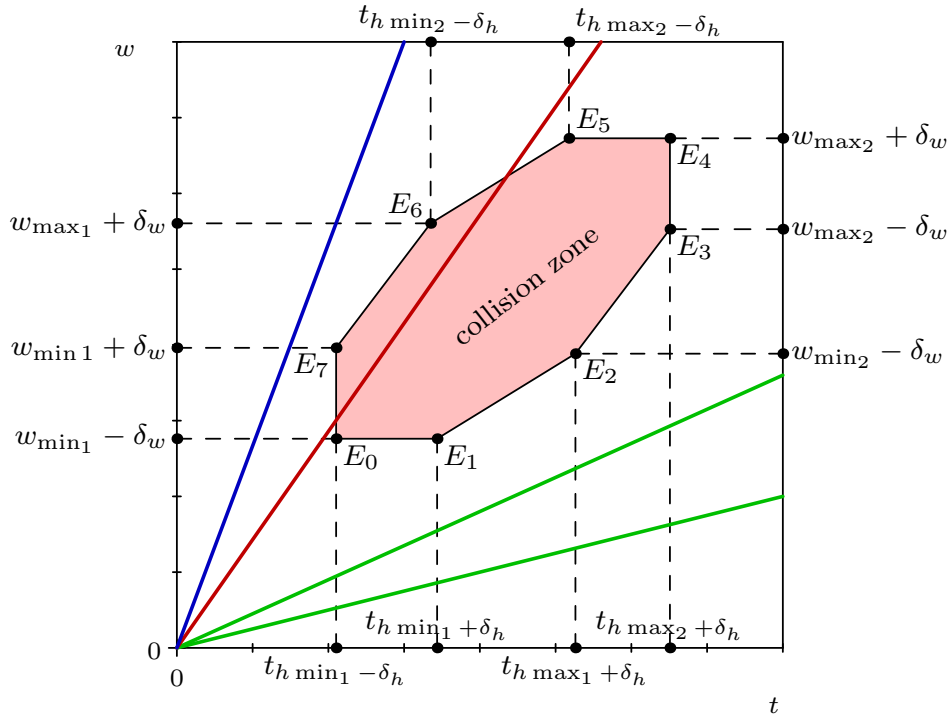


Figure 3.4: The velocity diagram for a single intersection of trajectories: the red area represents the collision zone in terms of space and time. Green lines are walker’s velocities that follow the pedestrian, red lines are walker’s velocities that will cause a collision, and blue lines are velocity that allow the walker to overtake the obstacle.

called  $ts = TimeStop(v_{0\alpha}^{(h)}, v_0^{(w)})$  and returns the minimum time required to wait to avoid the collision. This is clearly zero if  $\Delta T_h \cap \Delta T_w = \emptyset$ . After the amount of time  $ts$ , we can move with velocity  $v_0^{(w)}$  and be sure to avoid the obstacle.

Once we have fixed  $v_0^{(w)}$ , because we do not know what is the velocity  $v_{0\alpha}^{(h)}$  of the obstacle, we integrate over

all possible choices of  $v_{0\alpha}^{(h)}$ :

$$\int_{v_{0\min}^{(h)}}^{v_{0\max}^{(h)}} TimeStop(v_{0\alpha}^{(h)}, v_0^{(w)}) p_{\alpha}(v_{0\alpha}^{(h)}) dv_{0\alpha}^{(h)}. \quad (3.4)$$

In the planning phase we have to select the velocity  $v_0^{(w)}$  of the walker from a discrete set of values contained in  $[v_{0\min}^{(w)}, v_{0\max}^{(w)}]$ . We choose the value of  $v_0^{(w)}$  that minimises the overall cost computed with (3.4). In most of the cases the value of  $TimeStop$  will be zero, hence we select the  $v_0^{(w)}$  closest to a desired velocity  $v_d^{(w)}$ . This is written as

$$T = \arg \min_{v \in V} |v - v_d^{(w)}| \quad (3.5)$$

$$V = \arg \min_{v_0^{(w)}} \int_{v_{0\min}^{(h)}}^{v_{0\max}^{(h)}} TimeStop(v_{0\alpha}^{(h)}, v_0^{(w)}) p_{\alpha}(v_{0\alpha}^{(h)}) dv_{0\alpha}^{(h)} \quad (3.6)$$

With this technique we keep the walker on the established trajectory and we module only its velocity: if it is possible, we accelerate the walker in order to overtake the obstacle, if we do not have enough escaping velocity it is possible to slow down or stop and let the obstacle pass.

In the case of a cost  $T$  which is not acceptable (e.g. waiting time too high) or if it is not possible to stay on the current trajectory because of a colliding obstacle, we can perform a local re-planning of the current trajectory. This local deviation tries to reconnect smoothly to the original path, as explained next.

### 3.6 Local Re-planning

In the same way as proposed by different authors [18] and in our previous work [9], we advocate a strategy for trajectory re-planning based on a decomposition of the problem into geometric and dynamic planning. When a re-planning is requested, the algorithm selects a point  $P_0$  on the optimal trajectory with position  $(x_0, y_0)$ , angle  $\theta_0$ , curvature  $\kappa_0$  and speed  $v_0$  and a point  $P_2$ , with position  $(x_2, y_2)$ , angle  $\theta_2$ , curvature  $\kappa_2$ . The re-planned trajectory will depart from the old one at point  $P_0$  and will rejoin it at point  $P_2$ . Notably, the speed in  $P_2$  cannot be assigned, because, in general, it may not be reachable, e.g. if the global trajectory is time optimal. The algorithm seeks a new point  $P_1$  in the proximity of the obstacle to pivot on to find the best trajectory (see Figure 3.5). The connecting curve is a spline of clothoid curves [3] that exhibits  $C^2$  continuity with respect to the global trajectory, and that is very fast to compute. The different choices of point  $P_1$  can be explored via a deterministic search (as herein done) or by using stochastic methods. This strategy is computationally efficient with a new trajectory produced in a few milliseconds on standard architectures. In most of the reasonable application scenarios, the method reliably produces a solution. In the extreme cases in which it should not work, its efficiency leaves time to slow down the walker and back off to different emergency solutions. In principle, the algorithm presented below operates with any pair of entry and exit points  $P_0, P_2$  on the global trajectory. An obvious requirement is that  $P_0$  and  $P_2$  be located before and after the obstacle. The low computational cost of the algorithm allows us to test different possible choices or back off to an emergency strategy if the spline identified by the algorithm fails to satisfy the geometric or the dynamic constraints. However, the application of reasonable heuristics on the selection of  $P_0$  and  $P_2$  limits the occurrence of this anomaly. It is useful to observe that if the obstacle is very close to the walker, no feasible solution is likely to be found. On the other hand, if the obstacle is far away, we are in condition to generate a new global plan.

An intuitive and straightforward way to produce the points  $P_0$  and  $P_2$  is to identify them as the current position and at a distance which is reasonably far from the obstacle, respectively. Once a path is found, its validation is done with the previously described intersection techniques.

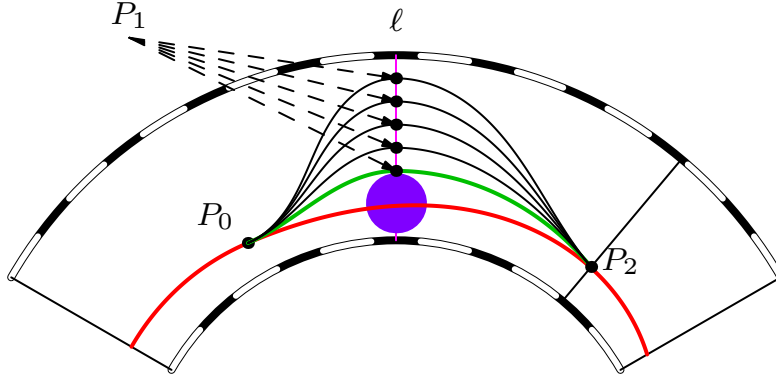


Figure 3.5: A sketch of the local re-planning method, in red the global trajectory that is no more feasible because of the obstacle (purple circle). In green the optimal escaping manoeuvre, in black feasible candidates for different choices of  $P_1$  located deterministically aside from the obstacle trajectory.

### 3.7 Reactive Re-planning

In this framework, where we already have the optimal trajectory, we compute the local re-planning that has to avoid the obstacle and connect with  $G^2$  continuity to the points  $P_0$  and  $P_2$  (e.g. Figure 3.5). For safety reasons, we first compute if it is possible to stop the vehicle before crashing into the obstacle while travelling on the assigned trajectory; after that we compute the reactive re-planning that tries to avoid the obstacle as in Figure 3.5. We require the following tools to compute the reactive re-planning, most of which are available in literature: a function for computing the time optimal speed profile for a given sequence of clothoids [8, 4, 9], and two functions that solve the  $G^1$  and  $G^2$  Hermite Interpolation Problem for clothoid curves (HIP). Those interpolation problems ask to find the parameters of a clothoid that interpolates the assigned initial and final points and angles, producing a spline that has geometric continuity up to the first derivative ( $G^1$  case). If also the curvature at the extremal points is specified, we say that it is a  $G^2$  HIP. Notice that in case of clothoids, which are parametrised by arc length, the geometric continuity ( $G^1$  and  $G^2$ ) is the same of the usual continuity (respectively  $C^1$  and  $C^2$ ). The notation with  $G$  is kept because it is traditional in this kind of problems. The  $G^1$  problem has been solved efficiently in [3], whereas the solution to the  $G^2$  problem is currently under review. For our scope it is sufficient to consider those solutions as two functions `g1Hip` and `g2Hip`, the latter corresponding to the solution of a nonlinear system of 16 equations that represent the continuity constraints. For instance, the  $G^2$  continuity between the segments connecting  $P_i$  to  $P_{i+1}$  requires that the following relations must hold:  $H_{i,j}(\theta_i, \kappa_i, \kappa'_i, L_i, \theta_{i+1}, \kappa_{i+1}) = 0$  for  $j = 0, 1, 2, 3$ , where

$$H_{i,0} := x_i + L_i X_0(\kappa'_i L_i^2, \kappa_i L_i, \theta_i) - x_{i+1}, \quad (3.7)$$

$$H_{i,1} := y_i + L_i Y_0(\kappa'_i L_i^2, \kappa_i L_i, \theta_i) - y_{i+1}, \quad (3.8)$$

$$H_{i,2} := \frac{1}{2} \kappa'_i L_i^2 + \kappa_i L_i + \theta_i - \theta_{i+1}, \quad (3.9)$$

$$H_{i,3} := \kappa'_i L_i + \kappa_i - \kappa_{i+1}. \quad (3.10)$$

Equations (3.7) and (3.8) ensure point-wise continuity, whereas (3.9) and (3.10) stand for the angle and curvature,  $X_0$  and  $Y_0$  are the functions defined in (2.14). The function `g2Hip` has to solve 4 of such blocks and can be evaluated relatively easily but only a limited number of times to keep the whole algorithm fast enough for real time applications.

We present now the geometric smooth connection of the escape manoeuvre to the optimal trajectory. The setting is the following: in  $P_0$  we know position, angle and curvature, as well as in  $P_2$ , in the middle point  $P_1$  we

know the position only, suitable angles and curvature should be found in order to connect  $P_0$  to  $P_1$  and  $P_1$  to  $P_2$  via the  $G^2$  HIP. For the sake of computational efficiency, we wish to call the g2Hip only twice, when the final interpolation is performed, and prefer instead to rely on the very fast g1Hip function to find the missing parameters, which costs 4 Newton iterations in the worst case (2 on average, see [3]). The idea is to construct two clothoid arcs neglecting the curvature at  $P_0$  and  $P_2$  but with  $G^2$  continuity at  $P_1$ . We use then the retrieved angle and curvature in  $P_1$  to interpolate from  $P_0$  to  $P_1$  and next to  $P_2$  maintaining  $G^2$  continuity with the assigned curvatures  $\kappa_0$  and  $\kappa_2$  by means of the function g2Hip.

We start connecting  $P_0$  to  $P_1$  with the function g1Hip, the  $G^1$  algorithm takes as input the points and angles to be interpolated and gives as output the curvatures  $\kappa'_0$ ,  $\bar{\kappa}_0$  and the length  $L_0$  of the clothoid. In our case g1Hip can thus be seen as a function of one unknown variable  $\theta_1$  because the other parameters are fixed, hence we obtain  $\kappa'_0(\theta_1)$ ,  $\bar{\kappa}_0(\theta_1)$  and  $L_0(\theta_1)$ . Analogously we perform the same calculations between  $P_1$  and  $P_2$  obtaining  $\kappa'_1(\theta_1)$ ,  $\kappa_1(\theta_1)$  and  $L_1(\theta_1)$ . Because  $\theta_1$  is the end angle of the first segment and the initial angle of the second segment, the resulting arcs match with  $G^1$  continuity in  $P_1$ . Thus, we have a family of splines made by two clothoids parametrised with  $\theta_1$  and we can vary this value in order to satisfy the  $G^2$  constraint, i.e. the curvatures of the two arcs in  $P_1$  must match. This condition is

$$h(\theta_1) := \kappa'_0(\theta_1)L_0(\theta_1) + \kappa_0(\theta_1) - \kappa_1(\theta_1) = 0, \quad (3.11)$$

which is simply equation (3.10) specialised to our scope. To find an angle  $\theta_1$  that satisfies  $h(\theta_1) = 0$  a standard Newton–Raphson scheme suffices, which works well in practice, and only 2-3 (cheap) iterations are required. The derivative of  $h(\theta_1)$  can be also explicitly written and is an expression that depends on already computed values. It can be easily evaluated by differentiating with respect to the angles  $\theta_i$  and  $\theta_{i+1}$  the three equations (3.7), (3.8), (3.9); the resulting linear relations for the desired derivatives are then solved straightforwardly. Even though the proof is simple, the explicit expressions of the results require some space and are herein omitted.

### 3.8 Group cohesion

An activity in ACANTO has the intention to provide therapeutic benefit and enjoyment for each user of the system. Therapy includes engaging in physical exercises. Enjoyment includes visiting places and seeing sights of interest. Social interaction with friends can provide both therapy and enjoyment, so activities are primarily intended for a group of participants. Thus the Reactive Planner should support motion tasks performed by both individuals and groups. Our proposed solution is to consider a single path as the global plan for the whole group involved in an activity. Each participant will then try to stay within some maximum distance of this path. That is, at any time we wish the participants to remain within a certain radius of the group centroid, without necessarily constraining them to a strictly specified path. We model this behaviour as a clothoid spline with a sufficiently wide offset, that is an appropriate clothoid tunnel.



## Chapter 4

### Example

As a concluding example we simulate the reactive replanning of the walker when it intersects the path of a pedestrian (Figure 4.1). The trajectory of the pedestrian is sampled from a real human and interpolated with clothoid arcs. The result is a  $G^2$  clothoid spline that minimizes the total jerk, as discussed in the ACANTO paper [5]. In Figure 4.1 (right) are shown all the candidates solutions for the re-planning. Their cost is depicted as a coloured segment ranging from red (high cost) to black (low cost). We can see that the chosen trajectory (in green) tries to pass behind the pedestrian. In Figure 4.2 there is a zoom of the region involved in the re-planning. In Figure 4.3 are shown the different velocities of the pedestrian in the velocity diagram previously discussed. Because the real velocity is not known exactly, but only as a probabilistic distribution, the optimal path is chosen minimizing the collision probability. If the resulting probability is higher than a fixed threshold for all the candidates trajectories, the Motion Execution Monitor raises an exception and calls the high level planner.

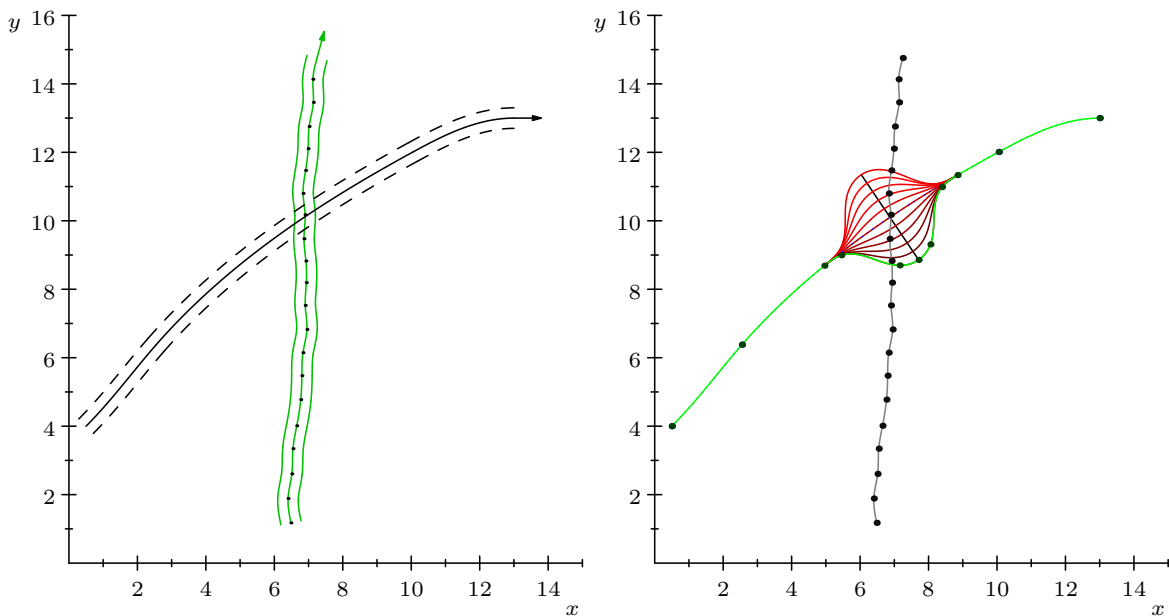


Figure 4.1: Left: In green the path of a pedestrian, in black the path of the walker. It is showed also the hindrance of both agents. There is a geometric collision. Right: Reactive re-planning of the walker's trajectory. Among the possible choices, the one with lowest cost is selected. Different costs are shown with different color gradations, ranging from red (maximum cost) to black (minimum cost). The green arc is the selected one.

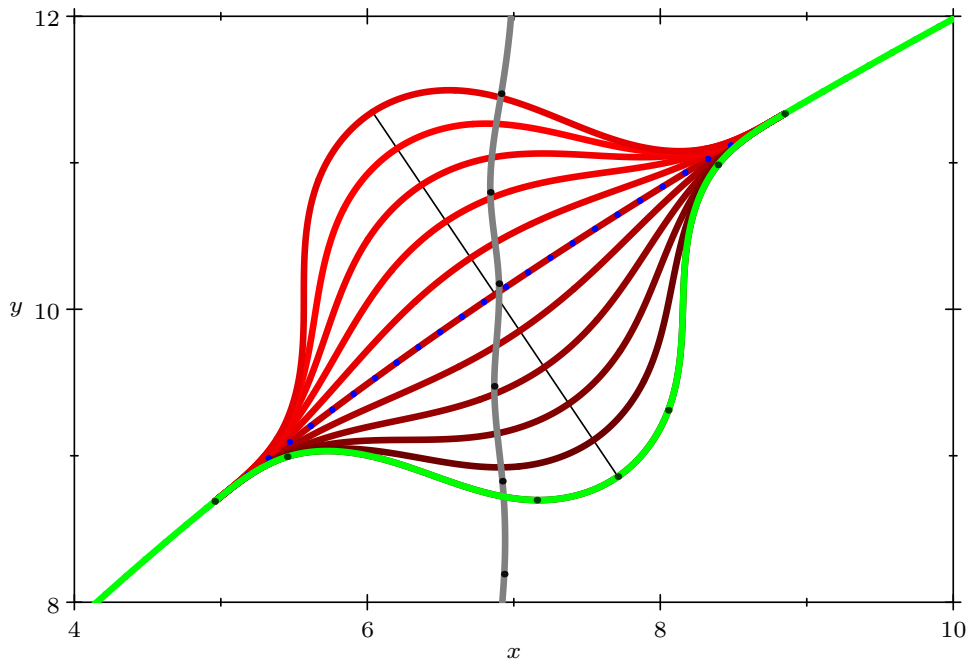


Figure 4.2: A zoom of the re-planning part of Figure 4.1 (right).

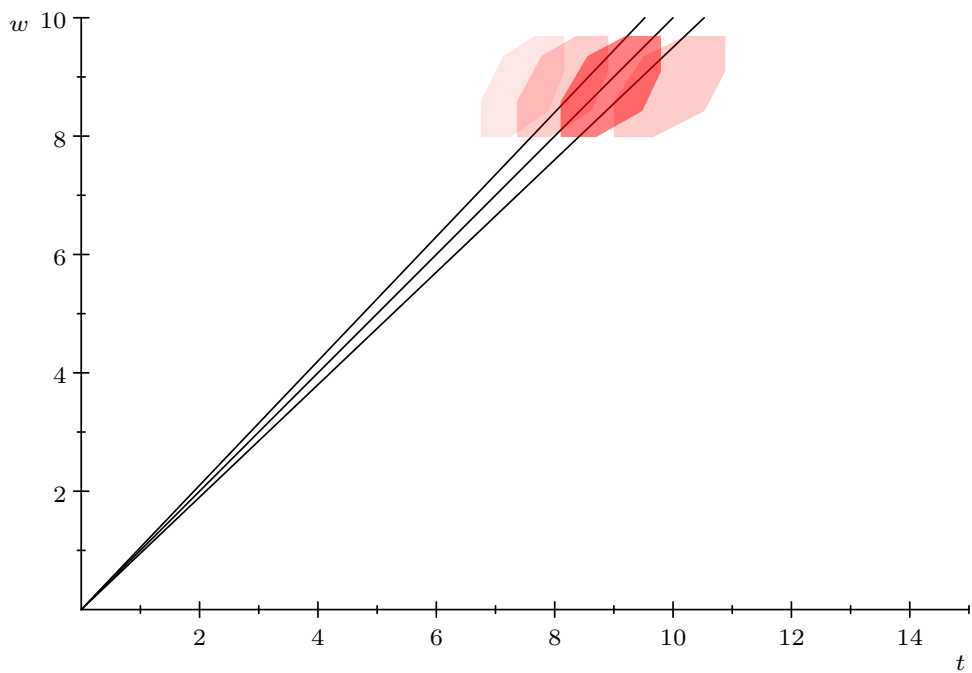


Figure 4.3: The velocity diagram for the original trajectory of the walker, with three available velocities  $v_0^{(w)}$  for the walker (black lines from the origin), and four probabilistic velocities  $v_{0\alpha}^{(h)}$  for the obstacle. The probability of each  $v_{0\alpha}^{(h)}$  is shown in red with different intensities.

## Chapter 5

### Link to other packages

The work presented in this deliverable has direct connections with other tasks of this work package and two main connections with other work packages. In fact, it is related with Task 5.3 - “Monitoring the execution of activities” since the same tool adopted for re-planning can be efficiently used to assess the adherence to the planned path and, in case, rise a flag of non conformity.

For what concerns the other work packages, it is related to WP2 - “Modelling” by means of the HSFM (Task 2.1 - “Models for social interaction”) that defines how the human beings sharing the space with the walker are supposed to move. Moreover, the definition of the control actions (Task 2.3 - “Logical representation of plans and control actions”) has an immediate impact on the way the re-planned trajectory are synthesised.

The second evident connection is with WP6 - “Design of Robotic Personal Devices”, since the guidance system is responsible of defining the type of trajectories that are actually feasible by the platform, hence limiting the choices of the re-planning manoeuvres. Notice that both WP2 and WP6 acts as input to this deliverable.



# Bibliography

- [1] G. Arechavaleta, J.-P. Laumond, H. Hicheur, and A. Berthoz. An optimality principle governing human walking. *IEEE Transactions on Robotics*, 24(1):5–14, Feb 2008.
- [2] Gustavo Arechavaleta, Jean-Paul Laumond, Halim Hicheur, and Alain Berthoz. On the nonholonomic nature of human locomotion. *Autonomous Robots*, 25(1-2):25–35, 2008.
- [3] Enrico Bertolazzi and Marco Frego. G1 fitting with clothoids. *Mathematical Methods in the Applied Sciences*, 38(5):881–897, 2015.
- [4] Enrico Bertolazzi and Marco Frego. Semi-analytical minimum time solution for the optimal control of a vehicle subject to limited acceleration. *Journal of Computational and Applied Mathematics (JCAM)*, 2016. Submitted.
- [5] P. Bevilacqua, M. Frego, E. Bertolazzi, D. Fontanelli, L. Palopoli, and F. Biral. Path planning maximising human comfort for assistive robots. In *2016 IEEE Conference on Control Applications (CCA)*, pages 1421–1427. IEEE, 2016.
- [6] Francesco Farina, Daniele Fontanelli, Andrea Garulli, Antonio Giannitrapani, and Domenico Prattichizzo. Walking ahead: The headed social force model. *PLOS ONE*, 12(1):1–23, 01 2017.
- [7] Gonzalo Ferrer and Alberto Sanfeliu. Proactive kinodynamic planning using the extended social force model and human motion prediction in urban environments. In *2014 IEEE/RSJ International Conference on Intelligent Robots and Systems*, pages 1730–1735. IEEE, 2014.
- [8] M. Frego, E. Bertolazzi, F. Biral, D. Fontanelli, and L. Palopoli. Semi-analytical minimum time solutions for a vehicle following clothoid-based trajectory subject to velocity constraints. In *2016 European Control Conference (ECC)*, pages 2221–2227, June 2016.
- [9] M. Frego, P. Bevilacqua, E. Bertolazzi, F. Biral, D. Fontanelli, and L. Palopoli. Trajectory planning for car-like vehicles: A modular approach. In *2016 IEEE 55th Conference on Decision and Control (CDC)*, pages 203–209, Dec 2016.
- [10] Ning Guo, Jian-Xun Ding, Xiang Ling, Qin Shi, and Imamura Takashi. The walking behavior of pedestrian crowd under impact of static and movable targets. *The European Physical Journal B*, 86(7), 2013.
- [11] Dirk Helbing, Illés Farkas, and Tamás Vicsek. Simulating dynamical features of escape panic. *Nature*, 407:487–490, September 2000.
- [12] Dirk Helbing and Peter Molnár. Social force model for pedestrian dynamics. *Phys. Rev. E*, 51:4282–4286, 1995.

- [13] Anders Johansson, Dirk Helbing, and Pradyumn K Shukla. Specification of the social force pedestrian model by evolutionary adjustment to video tracking data. *Advances in Complex Systems*, 10(supp02):271–288, 2007.
- [14] Katja Mombaur, Anh Truong, and Jean-Paul Laumond. From human to humanoid locomotion – an inverse optimal control approach. *Autonomous robots*, 28(3):369–383, 2010.
- [15] S. Okazaki. A study of simulation model for pedestrian movement in architectural space. Part 1: Pedestrian movement by the application of magnetic model. *Transactions of Architectural Institute of Japan*, 283:111–119, 1979.
- [16] Quang-Cuong Pham, Halim Hicheur, Gustavo Arechavaleta, Jean-Paul Laumond, and Alain Berthoz. The formation of trajectories during goal-oriented locomotion in humans. ii. a maximum smoothness model. *European Journal of Neuroscience*, 26(8):2391–2403, 2007.
- [17] PradyumnKumar Shukla. On Modeling and Evolutionary Optimization of Nonlinearly Coupled Pedestrian Interactions. In *Applications of Evolutionary Computation*, volume 6024 of *Lecture Notes in Computer Science*, pages 21–30. Springer Berlin Heidelberg, 2010.
- [18] E. Velenis and P. Tsiotras. Minimum-time travel for a vehicle with acceleration limits: Theoretical analysis and receding-horizon implementation. *Journal of Optimization Theory and Applications*, 138(2):275–296, 2008.
- [19] W. J. Yu, R. Chen, L. Y. Dong, and S. Q. Dai. Centrifugal force model for pedestrian dynamics. *Phys. Rev. E*, 72:026112, Aug 2005.
- [20] Jing Zhao, Yi Xu, Xiaokang Yang, and Qing Yan. Crowd instability analysis using velocity-field based Social Force Model. In *IEEE Visual Communications and Image Processing (VCIP)*, pages 1–4, Nov 2011.